Bulk Superconductivity in Pressurized Trilayer Nickelate $Pr_4Ni_3O_{10}$ Single Crystals

Enkang Zhang [1,2,*] Di Peng,[3,*] Yinghao Zhu [1,*] Lixing Chen,[1] Bingkun Cui [1] Xingya Wang,[4]
Wenbin Wang,[5] Qiaoshi Zeng [3,6,†] and Jun Zhao [1,2,5,7,‡]

[1]*State Key Laboratory of Surface Physics and Department of Physics, Fudan University,*
Shanghai 200433, China
[2]*Shanghai Research Center for Quantum Sciences, Shanghai 201315, China*
[3]*Shanghai Key Laboratory of Material Frontiers Research in Extreme Environments (MFree),*
Shanghai Advanced Research in Physical Sciences (SHARPS), Shanghai 201203, China
[4]*Shanghai Synchrotron Radiation Facility, Shanghai Advanced Research Institute,*
Chinese Academy of Sciences, Shanghai 201204, China
[5]*Institute of Nanoelectronics and Quantum Computing, Fudan University, Shanghai 200433, China*
[6]*Center for High Pressure Science and Technology Advanced Research, Shanghai 201203, China*
[7]*Hefei National Laboratory, Hefei 230088, China*

The discovery of superconductivity in pressurized bilayer and trilayer nickelates has generated significant interest. However, their superconducting properties are often dependent on sample quality and pressure conditions, complicating the interpretation of the underlying physics. Finding new systems with optimized bulk superconducting properties is therefore important for advancing our understanding of these materials. Unlike cuprates, where trilayer compounds typically exhibit the highest transition temperature (T_c), the bilayer nickelate $La_3Ni_2O_7$ has thus far outperformed the trilayer $La_4Ni_3O_{10}$ in reported T_c. Whether the trilayer nickelates have achieved the optimal T_c remains unclear, with various scenarios suggesting different possibilities. Here, we report the discovery of bulk superconductivity in pressurized $Pr_4Ni_3O_{10}$ single crystals, achieving a maximum onset T_c of 40.5 K at 80.1 GPa, significantly exceeding the 30 K observed in $La_4Ni_3O_{10}$. The bulk nature of superconductivity is confirmed by zero resistance and a strong diamagnetic response below T_c, with a superconducting volume fraction exceeding 80%. These findings establish trilayer nickelates as genuine bulk high-temperature superconductors, provide new insights into the mechanisms driving superconductivity, and point to a promising route toward further enhancing superconducting properties in nickelates.

Subject Areas: Condensed Matter Physics,
Strongly Correlated Materials,
Superconductivity

I. INTRODUCTION

High-temperature (high-T_c) superconductivity has fascinated condensed-matter physicists and materials scientists, offering both technological applications and fundamental insights into strongly correlated electron systems [1–3]. Since the discovery of high-T_c cuprates more than three decades ago, the search for new families of superconductors has remained a central focus in this field [4–6].

Nickel-based materials have long been proposed as promising candidates for replicating the high-temperature superconductivity observed in cuprates [7]. This interest led to the discovery of superconductivity in infinite-layer nickelates [8], which share important structural and electronic similarities with cuprates. Recently, Ruddlesden-Popper (RP) phase bilayer nickelate $La_3Ni_2O_7$ was shown to exhibit superconductivity under high pressures, with transition temperatures (T_c) approaching 80 K [9–11]. This unexpected finding prompted discussions about the underlying mechanisms of superconductivity, including analogies to cuprates and the potential for multiorbital physics that goes beyond simple cupratelike models [12].

Despite these advances, challenges remain in fully understanding the superconducting properties of nickelates under pressure. Notably, superconductivity in these

*These authors contribute equally to this work.

†Contact author: zengqs@hpstar.ac.cn.

‡Contact author: zhaoj@fudan.edu.cn.

materials is often sensitive to sample quality and pressure conditions, and the superconducting volume fractions are frequently low [13–16]. These sample-dependent variations hinder the identification of the precise mechanisms governing superconductivity in nickelates and raise fundamental questions about the nature of the superconducting phase in these materials.

Very recently, studies have revealed that trilayer nickelate $La_4Ni_3O_{10}$ single crystals host bulk superconductivity with rather high superconducting volume fractions of around 86% under pressure [17]. Drawing from analogies with cuprates, where trilayer systems often achieve the highest T_c [18–20], it was anticipated that $La_4Ni_3O_{10}$ might exhibit an even higher T_c than $La_3Ni_2O_7$. However, experimental reports on pressurized $La_4Ni_3O_{10}$ indicate a T_c ranging from 20 to 30 K [17,21–23], substantially below the 80 K observed for $La_3Ni_2O_7$. These observations raise fundamental questions about whether trilayer nickelates have yet reached their intrinsic superconducting potential or if additional tuning strategies are necessary to optimize their electronic and structural properties.

A promising strategy for tuning superconductivity in RP phase nickelates involves inducing "internal chemical pressure" through chemical substitution of rare-earth ions [24,25]. These substitutions may alter lattice constants, bond lengths, or angles, thereby modifying the electronic environment without introducing extra disorder on the NiO_2 plane. By introducing internal chemical pressure, in combination with applied hydrostatic pressure, it may be possible to explore superconductivity in new dimensions in nickelates.

II. RESULTS

In this work, we investigate the trilayer nickelate $Pr_4Ni_3O_{10}$ single crystals under ambient and high-pressure conditions. Polycrystalline samples were synthesized using conventional solid-state methods, followed by pressing the material into precursor rods and sintering them in an air atmosphere. High-quality single crystals of $Pr_4Ni_3O_{10}$ were subsequently grown from the sintered rods using a high-pressure vertical optical floating-zone furnace (see Sec. V). X-ray diffraction (XRD) measurements on cleaved surfaces of $Pr_4Ni_3O_{10}$ crystals revealed sharp $(0\,0\,L)$ Bragg peaks, consistent with a trilayer structure [Fig. 1(a) in Supplemental Material [26]]. Further Rietveld refinements of x-ray diffraction data from powdered single crystals confirmed a trilayer structure similar to that of $La_4Ni_3O_{10}$ but with reduced lattice parameters [see Fig. 1(b) and Table 1 in Supplemental Material [26]]. This reduction suggests the influence of internal chemical pressure resulting from the smaller ionic radius of Pr^{3+} compared to La^{3+}. The refined crystal structure belongs to the monoclinic $P2_1/a$ space group [Figs. 1(a) and 1(b)], consistent with previous studies [27,28].

To explore the structural evolution of $Pr_4Ni_3O_{10}$ under pressure, we conducted synchrotron x-ray diffraction measurements on powdered single crystals. At low pressures, the data confirm a monoclinic $P2_1/a$ structure [Figs. 1(a) and 1(b)]. Upon increasing the pressure above 35 GPa, a structural transition to the tetragonal $I4/mmm$ phase is observed, as evidenced by the merging of the (020) and (200) diffraction peaks [Figs. 1(c), 1(f), and 1(g)]. These findings are analogous to those reported for $La_4Ni_3O_{10}$, although $Pr_4Ni_3O_{10}$ exhibits a notably higher transition pressure [17]. Our refinements reveal that the Ni−O−Ni bonding angle between adjacent NiO_2 layers increases from 161.4° to 180° during this phase transition [Figs. 1(a), 1(d), and 1(e)]. This change indicates that the enhancement of interlayer coupling under pressure is likely a universal feature of trilayer nickelates.

Thermodynamic measurements were also conducted at ambient pressure. The heat capacity data exhibit a sharp peak at $T_d = 157$ K, indicating the onset of density-wave ordering [Fig. 2(a)], which involves an intertwined spin and charge density wave [29]. In addition to the density-wave transition at 157 K, the heat capacity data also show an anomaly around 5 K, likely corresponding to the development of magnetic order of the Pr moments (Fig. 2 in Supplemental Material [26]) [27,28].

Concurrently, magnetic susceptibility measurements exhibit a subtle anomaly at $T_d = 157$ K [Fig. 2(b)], which can be seen more clearly in the derivative of the susceptibility plot. Notably, the susceptibility anomaly at T_d is much weaker than that observed in $La_4Ni_3O_{10}$ [17], which is likely because the transition is masked by the dominated paramagnetic susceptibility from Pr^{3+} local moments.

To explore the transport properties under pressure, resistance measurements were conducted up to 80.1 GPa using diamond anvil cells (DAC). Because of the extreme sensitivity of superconducting properties to pressure conditions in ceramiclike materials such as nickelates, cuprates, and chromium arsenides [10,17,30], helium was utilized as the pressure-transmitting medium to ensure ideal hydrostatic conditions. At ambient pressure, the resistance of $Pr_4Ni_3O_{10}$ exhibits metallic behavior with a sharp kink corresponding to $T_d = 157$ K [Fig. 2(c)]. Upon increasing the pressure to 33.1 GPa, the anomaly associated with T_d becomes weakened and shifts to 89 K, while a pronounced decrease in resistance emerges below approximately 25 K, signaling the onset of a superconducting transition [Fig. 3(a)]. As the pressure is further increased, the density-wave order diminishes, and T_c continues to rise, achieving zero resistance above 48.9 GPa [Fig. 3(a) and 3(b)]. Ultimately, at a pressure of 80.1 GPa, the superconducting onset temperature reaches around 40.5 K [Fig. 3(a)], significantly higher than the 20–30 K reported for $La_4Ni_3O_{10}$ [17].

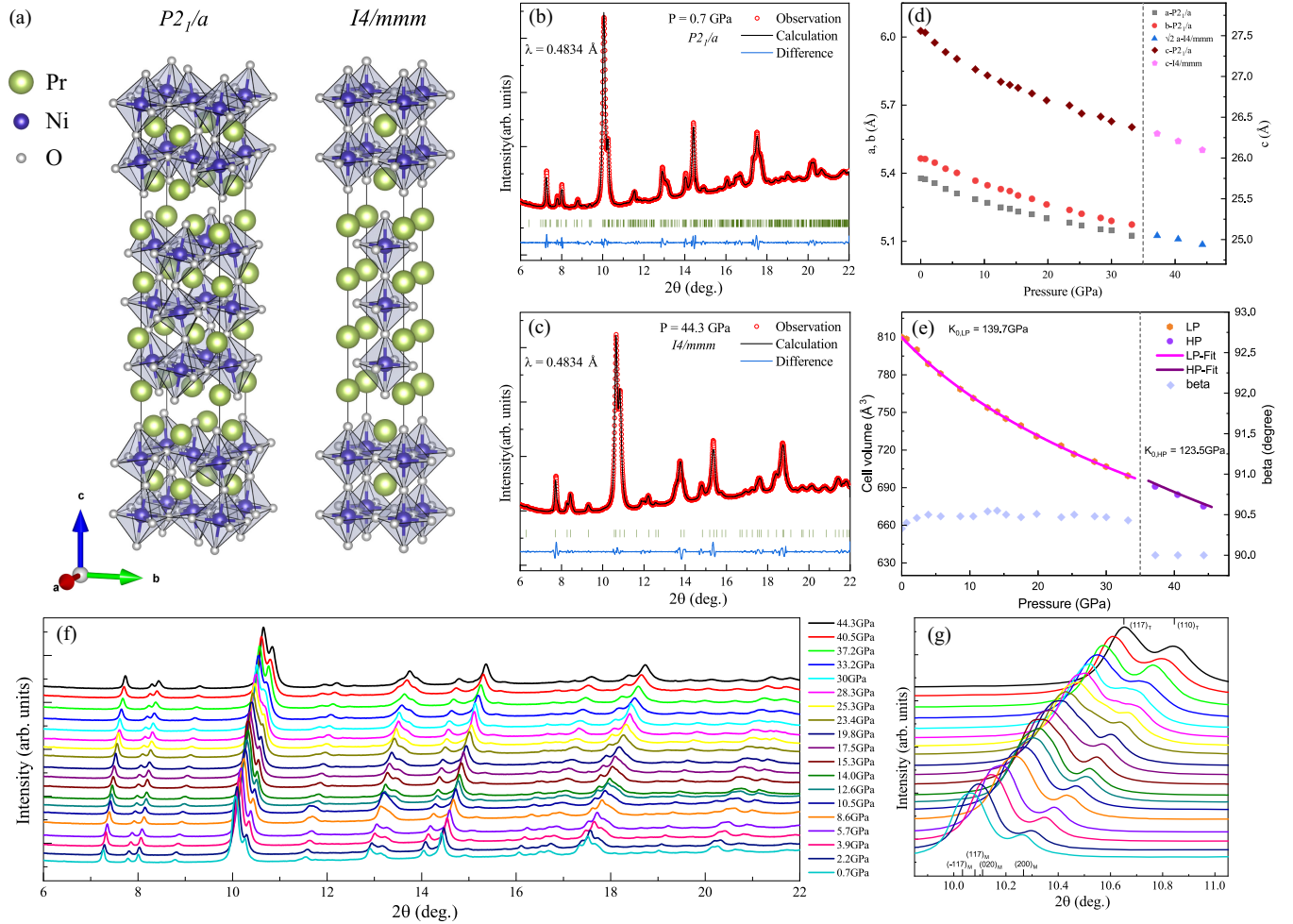To clarify the evolution of the density-wave order and superconductivity under pressure in more detail,

FIG. 1.   (a) Crystal structure of $Pr_4Ni_3O_{10}$ at ambient and low pressure (< 35 GPa, left) and high pressure (> 35 GPa, right). (b),(c) Rietveld refinements of synchrotron-based powder XRD pattern of $Pr_4Ni_3O_{10}$ at 0.7 GPa and 44.3 GPa at room temperature, respectively. (d) Pressure-dependent lattice constants a, b, and c determined from the Rietveld refinements. (e) Pressure dependence of the cell volume and β angle obtained from Rietveld refinements, with the solid line representing a fit to the third-order Birch-Murnaghan equation of state, illustrating the compression behavior of the unit cell. (f) Overall view of room-temperature synchrotron XRD patterns of pressurized $Pr_4Ni_3O_{10}$ ranging from 0.7 GPa to 44.3 GPa with a wavelength λ of 0.4834 Å. (g) Enlarged view of diffraction peaks within the range of $9.85° \leq 2\theta \leq 11.05°$, illustrating the merging of the monoclinic $(020)_M$ and $(200)_M$ peaks into the tetragonal $(110)_T$ peak, and indicating a structural phase transition from monoclinic to tetragonal.

we carefully prepared another sample in a helium DAC with optimized hydrostaticity. This careful loading allows for a clearer observation of the density-wave and superconducting transitions, showing an onset superconducting transition T_c of 40.2 K and a zero-resistance T_c of 24 K at 56.7 GPa (Fig. 4), both significantly higher than those in $La_4Ni_3O_{10}$ [17]. These results confirm that the observed effects are reproducible.

Interestingly, the normal-state resistance of $Pr_4Ni_3O_{10}$ deviates from conventional metallic behavior, following a power-law relationship $\rho(T) = \rho_0 + AT^n$ with an exponent n ranging from 1 to 1.5, depending on the pressure and temperature range fitted [Figs. 3(a) and 4(a)]. An exponent smaller than 2 suggests non-Fermi liquid behavior, potentially induced by strong electron

correlations or spin fluctuations near a quantum critical point. This behavior is somewhat different from that of $La_4Ni_3O_{10}$, where a linear temperature dependence of resistance is observed in the normal state near the pressure range of optimal T_c [17]. The difference between $La_4Ni_3O_{10}$ and $Pr_4Ni_3O_{10}$ may be related to the influence of the Pr^{3+} local moments. Future studies should explore this discrepancy further.

Figure 3(c) illustrates the effects of an external magnetic field on the temperature-dependent resistance of $Pr_4Ni_3O_{10}$. Under an applied magnetic field perpendicular to the ab plane, the superconducting transition is progressively suppressed, which provides further confirmation that the observed transition is indeed due to superconductivity. The suppression of superconductivity with increasing
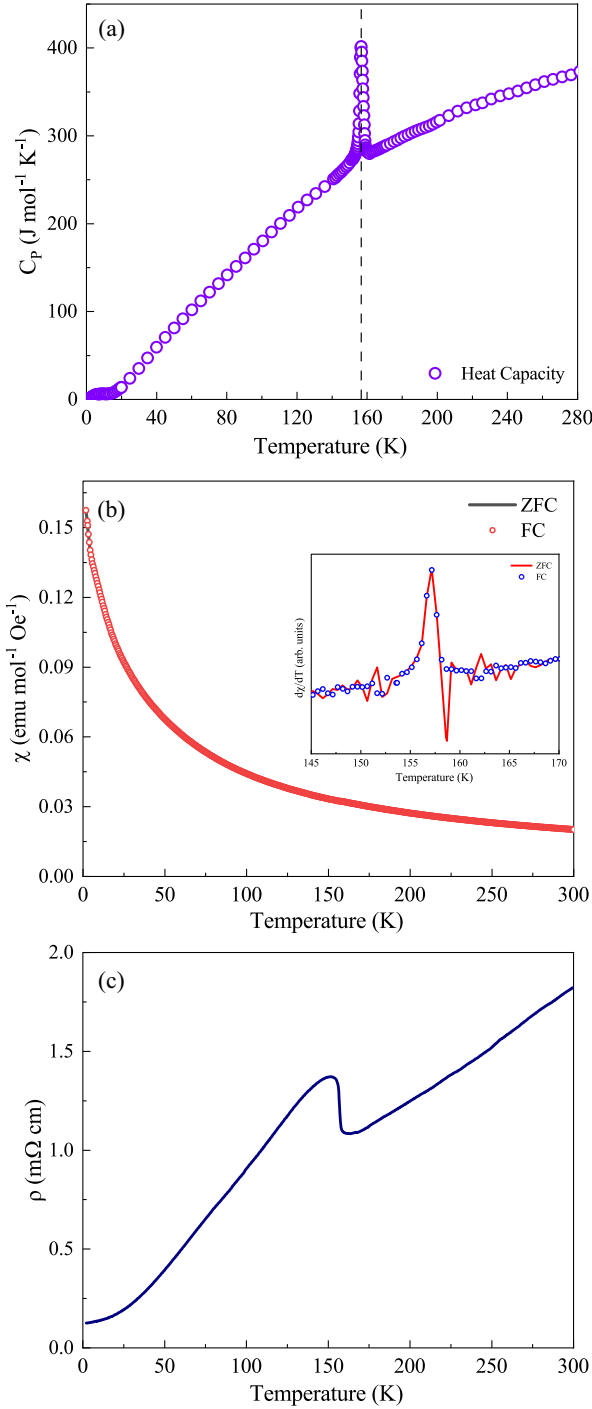
FIG. 2. (a) Specific heat (C_p) of a $Pr_4Ni_3O_{10}$ single crystal measured from 1.8 K to 280 K. The density-wave order transition characterized by a sharp peak in the C_p curve occurs at $T_d = 157$ K. (b) Magnetic susceptibility (χ) of the $Pr_4Ni_3O_{10}$ single crystal measured from 1.8 K to 300 K with an applied field of 0.5 T, parallel to the *ab* plane. The inset shows the derivative of susceptibility, $d\chi/dT$. (c) Resistance profile of the $Pr_4Ni_3O_{10}$ single crystal in the *ab* plane at ambient pressure.

magnetic field can be described by Ginzburg-Landau (GL) theory, using the relationship

$$H_{c2}(T) = H_{c2}(0)[(1 - t^2)/(1 + t^2)],$$

where $t = T/T_c$ is the reduced temperature and T_c is defined as the temperature at which the resistance reaches 90% of its normal state value near the onset of superconductivity. By fitting the experimental data to this GL form, we obtained an upper critical field H_{c2} of approximately 53 T at 75.1 GPa [Fig. 3(d)]. This value exceeds the upper critical fields reported for $La_4Ni_3O_{10}$, highlighting the enhanced superconducting robustness of $Pr_4Ni_3O_{10}$ under high pressure. Moreover, our calculation of the in-plane superconducting coherence length for $Pr_4Ni_3O_{10}$ at 75.1 GPa is about 25 Å. The short superconducting coherence length suggests that the Cooper pairs are spatially confined, pointing to strong electron pairing interactions similar to those found in other high-temperature superconductors [2,3,31].

To further substantiate the intrinsic nature of superconductivity in $Pr_4Ni_3O_{10}$, we performed dc magnetic susceptibility measurements under high pressures using a custom-built Be-Cu alloy miniature DAC. Neon was employed as the pressure-transmitting medium to ensure optimal hydrostatic conditions. In the raw zero-field-cooled (ZFC) susceptibility data at 40.2 GPa, strong diamagnetic signals were clearly observed below T_c, confirming the presence of the Meissner effect [Fig. 5(a)]. When the pressure was increased to 49.5 GPa (the upper limit achievable in our miniature cell), T_c rose [Fig. 5(b)]. This pressure-induced increase in T_c is consistent with trends observed in resistance measurements. Together, these susceptibility and resistance data unambiguously confirm that the observed transition is due to superconductivity.

Furthermore, analysis of the dc magnetic susceptibility data revealed superconducting volume fractions of approximately 85% at 40.2 GPa and 88% at 49.5 GPa, after correcting for the demagnetizing factor associated with the sample geometry (see Sec. V, as well as Fig. 3 in Supplemental Material [26]). These substantial superconducting volume fractions demonstrate that superconductivity is an intrinsic bulk property of the $Pr_4Ni_3O_{10}$ phase, rather than arising from minor secondary phases or filamentary regions.

Figure 5(c) summarizes the structural evolution, density-wave order, and superconductivity phase diagram of $Pr_4Ni_3O_{10}$ under pressure. The results reveal that pressure suppresses the density-wave order and induces superconductivity, a behavior analogous to other high-temperature superconductors. Additionally, a monoclinic-to-tetragonal phase transition is observed at around 35 GPa, which is
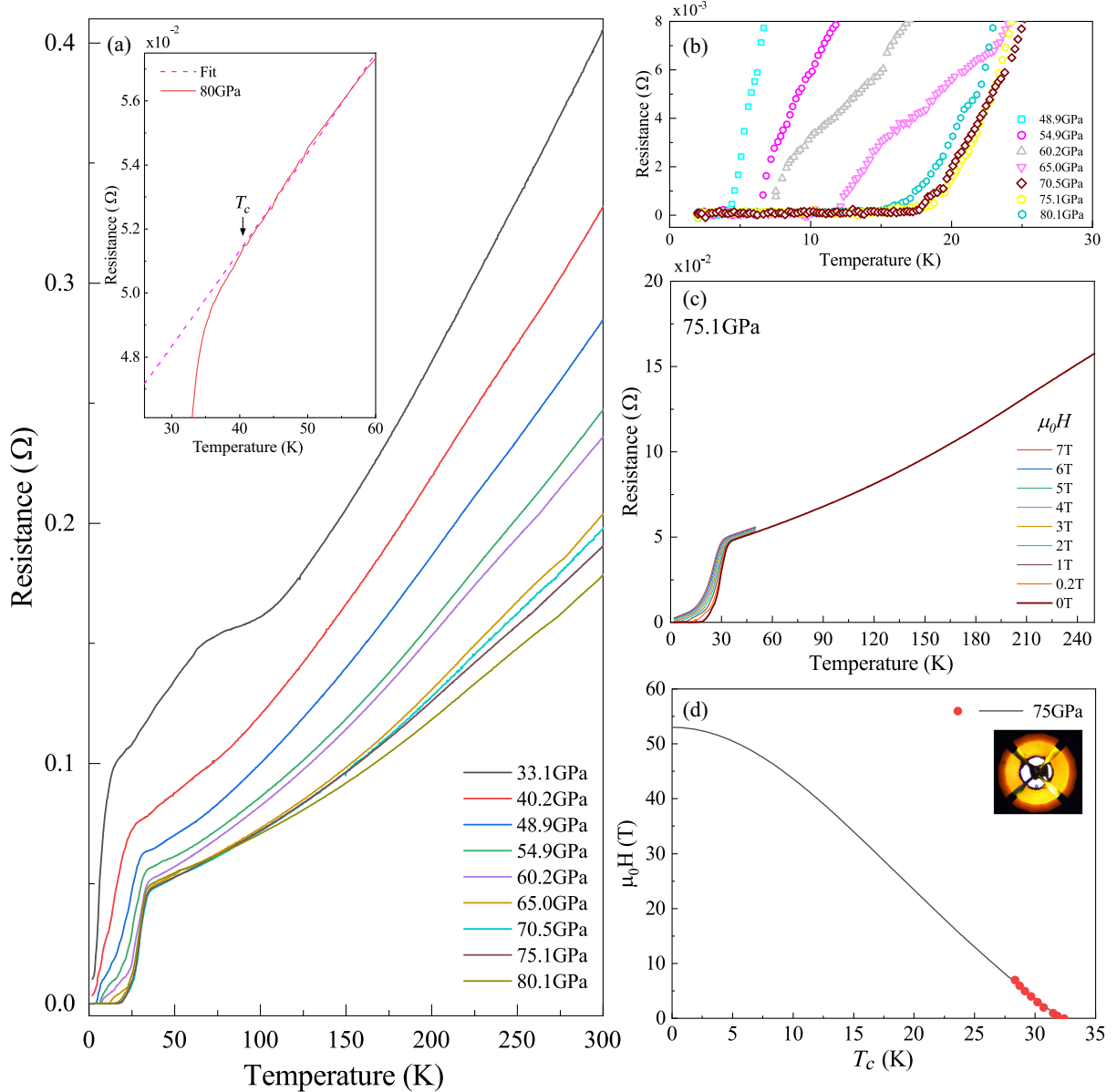
FIG. 3.   (a) Resistances of the $Pr_4Ni_3O_{10}$ single crystal at pressures ranging from 33.1 GPa to 80.1 GPa in the helium DAC for sample S1. The inset shows the onset $T_c = 40.5$ K, which is defined as the temperature at which the $R - T$ curve deviates from a power-law $\rho(T) = \rho_0 + AT^n$ fit. (b) Enlarged view of the resistance curve near zero resistivity. (c) Magnetic field effects on the superconducting transition in $Pr_4Ni_3O_{10}$ at 75.1 GPa. The magnetic fields are applied perpendicular to the ab plane. (d) Ginzburg-Landau fittings of the upper critical fields at 75.1 GPa. The inset shows a photograph of the electrodes used for high-pressure resistance measurements.

notably higher than that (13–15 GPa) observed in $La_4Ni_3O_{10}$ [17].

III. DISCUSSION

The markedly higher T_c observed in $Pr_4Ni_3O_{10}$ compared to $La_4Ni_3O_{10}$ provides important insight into the mechanism driving nickelate superconductivity. Unlike conventional doping, substituting Pr^{3+} for La^{3+} does not induce extra carrier doping or disorder; rather, the smaller ionic radius of Pr^{3+} generates internal chemical pressure,

reducing the lattice constants and the c/a ratio [17]. This lattice-parameter modification appears to enhance exchange couplings, which has been proposed by theory as the primary driver of electron pairing in nickelates [25,32]. In particular, these theoretical studies suggest that substituting smaller rare-earth ions strengthens interlayer exchange coupling through structural modifications, thereby boosting the pairing energy and ultimately increasing T_c, which is consistent with our experiments. Collectively, these observations point to a strong interplay between structural tuning and superconductivity in
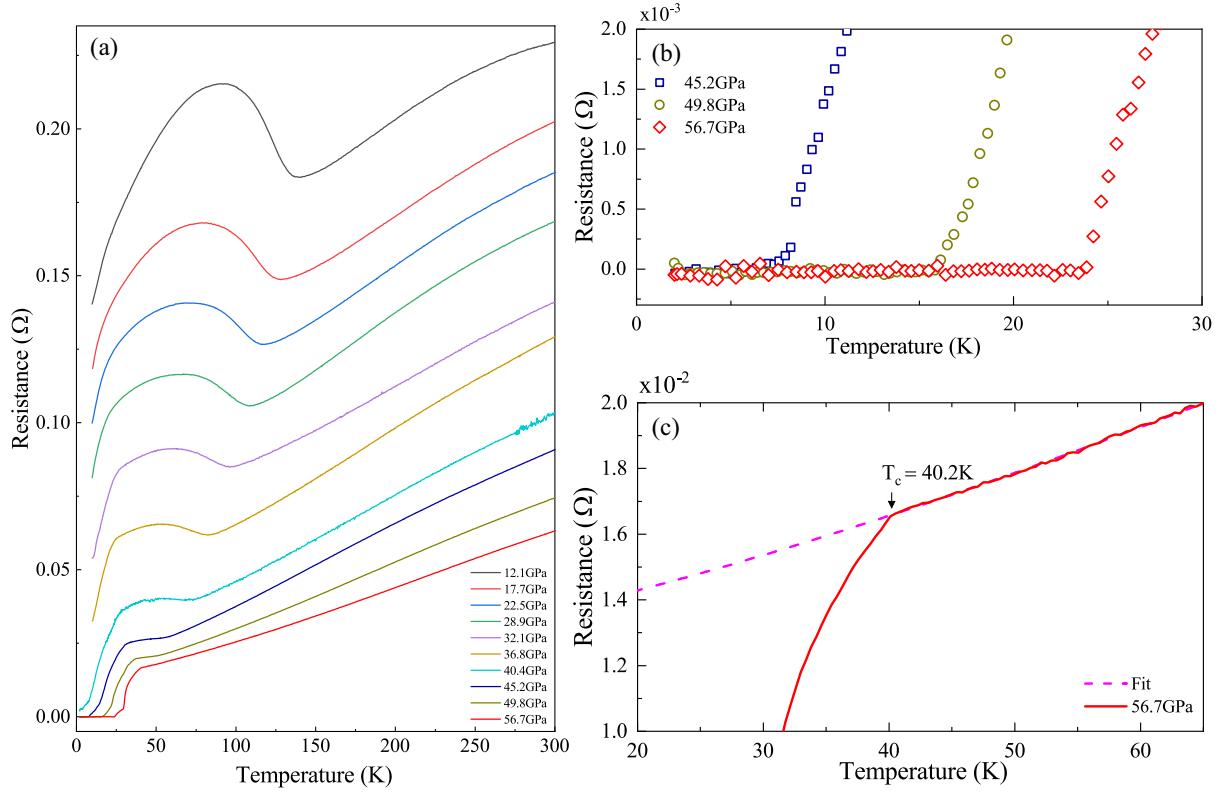
FIG. 4. (a) Resistances of the $Pr_4Ni_3O_{10}$ single-crystal sample S4 at pressures ranging from 12.1 GPa to 56.7 GPa in a helium DAC. The sample was carefully loaded to optimize hydrostaticity, allowing for a clear observation of the evolution of the density-wave transition and superconducting transition. (b) Enlarged view of the resistance curve near zero resistance. (c) Enlarged view of the resistance of sample S4 at 56.7 GPa near the onset T_c. The dashed line represents a fit using the $\rho(T) = \rho_0 + AT^n$ equation, indicating an onset T_c of 40.2 K.
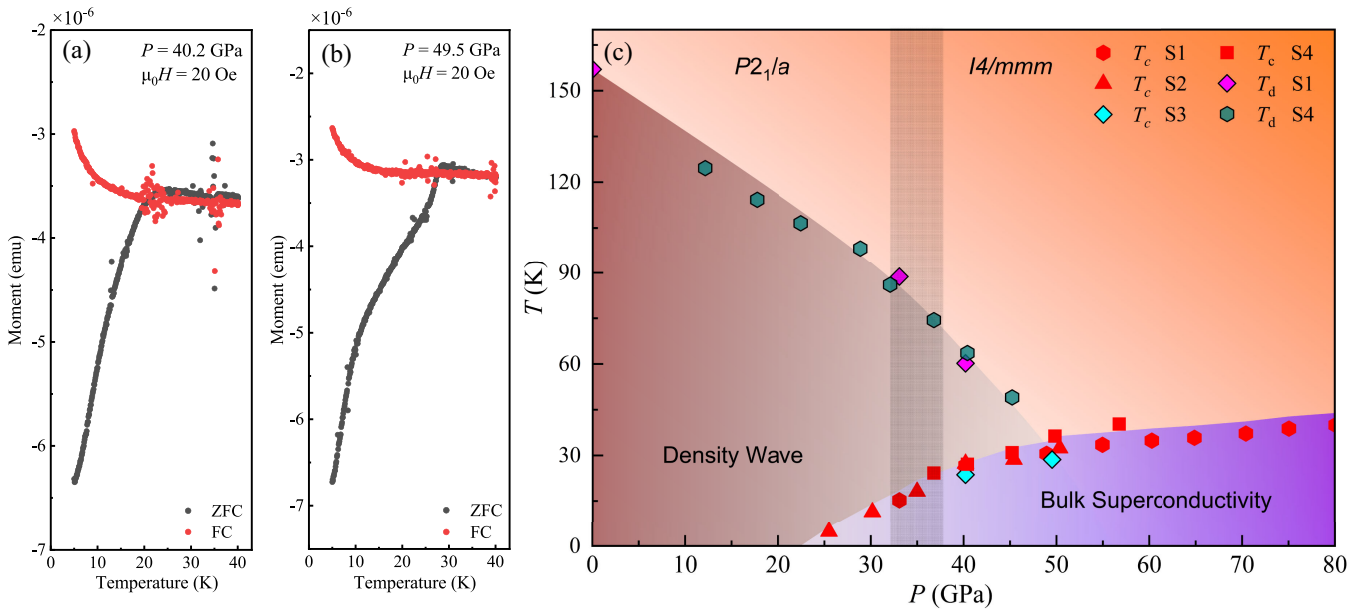

FIG. 5. (a),(b) Temperature-dependent dc susceptibilities of $Pr_4Ni_3O_{10}$ single crystals under various pressures. Both ZFC and field-cooled (FC) measurement modes were applied. Distinct superconducting diamagnetic responses below T_c are observed in ZFC curves for 40.2 GPa (a) and 49.5 GPa (b). (c) Phase diagram of $Pr_4Ni_3O_{10}$ under pressure. The red solid hexagons, triangles, and squares represent the $T_{c\,\text{onset}}$ of samples S1, S2, and S4 of the resistance curve in the helium DAC, respectively. The blue diamonds and teal hexagon denote the density-wave transition T_d of S1 and S4 determined from the anomaly in the resistance curve. The turquoise diamonds denote the T_c of samples S3 defined by magnetic susceptibility in the neon DAC.

nickelates, highlighting the idea that targeted chemical substitutions aimed at enhancing exchange coupling can be an effective strategy for improving superconductivity.

Furthermore, the reduced ionic radius of Pr^{3+} could increase the three dimensionality of the electronic structure. In cuprates, the enhanced three dimensionality may not be helpful for superconductivity as it reduces quantum fluctuations. However, in nickelates, the situation may differ. It has been proposed that interlayer coupling involving d_{z^2} bands, which are inherently more three dimensional than $d_{x^2-y^2}$ bands [33–36], plays a crucial role in the pairing mechanism [32,37–41]. Consequently, increased three dimensionality and enhanced interlayer coupling could be favorable for superconductivity in nickelates. This idea aligns with the observed monoclinic-to-tetragonal phase transition, which enhances interlayer coupling and is accompanied by the appearance of superconductivity in this system. Indeed, it has been shown that $Pr_4Ni_3O_{10}$ exhibits rather weak anisotropy between in-plane and out-of-plane resistances [27].

These analyses suggest that similar trends may apply to other nickelate superconductors and offer an effective pathway for enhancing superconductivity by substituting smaller rare-earth elements—such as Nd, Sm, and Gd—in both bilayer and trilayer nickelates. However, it should be noted that when extremely large internal pressures are applied, the increased orbital overlap and hopping between nearest neighbors become more pronounced, potentially broadening the electronic bandwidth, which could reduce electronic correlations and weaken pairing strength [24]. Therefore, an optimal superconducting regime likely exists, where exchange couplings and electron correlations are finely balanced. Following this approach, by combining rare-earth doping with external pressure, and possibly with substrate strain [42,43], further enhancement of superconductivity in nickelates could be achieved, potentially even under ambient or low pressures.

IV. CONCLUSION

In summary, our experiments demonstrate that $Pr_4Ni_3O_{10}$ exhibits robust bulk superconductivity under high pressure, achieving transition temperatures up to 40.5 K at 80.1 GPa, which is substantially higher than the 30 K observed in its La-based counterpart. This significant enhancement underscores the critical role of internal chemical pressure, induced by the smaller ionic radius of Pr^{3+}, in enhancing magnetic interactions essential for high-temperature superconductivity. Moreover, the substantial superconducting volume fraction of approximately 88% affirms that superconductivity in $Pr_4Ni_3O_{10}$ is an intrinsic bulk property, rather than contributions from secondary phases or filamentary regions. The 30% increase in T_c through Pr substitution suggests that further chemical substitutions with smaller rare-earth ions could open the door to discovering superconductors with even higher T_c

values, in both trilayer and bilayer configurations, thereby pushing the boundaries of superconducting performance in nickelates.

V. METHODS

A. Growth of $Pr_4Ni_3O_{10}$ single crystals

The synthesis of the precursor powder for the $Pr_4Ni_3O_{10}$ compound was conducted using a conventional solid-state reaction approach. Pr_6O_{11} (Aladdin, 99.99%) and NiO (Aladdin, 99.99%) were used as raw materials, with an additional 0.5% NiO added to compensate for potential volatilization during crystal growth. Before weighing, the Pr_6O_{11} powder was dried to eliminate moisture absorbed during storage. Subsequently, the mixture was finely ground and mixed, followed by calcination at 1373 K for 24 hours, with two repeated cycles to ensure complete and homogeneous reactions.

The powder was subsequently pressed into polycrystalline rods (approximately 12 cm in length and 6 mm in diameter) under a hydrostatic pressure of 70 MPa for 30 minutes. These rods were then sintered at 1673 K for 12 hours in air. Single crystals were cultivated utilizing a vertical optical-image floating-zone furnace (Model HKZ, SciDre) at Fudan University. The rod was initially traversed through the growth zone at a rapid speed of 20 mm h^{-1} and 10-bar oxygen pressure to enhance density; then, the growth was carried out at a growth rate of 2 mm h^{-1} within an oxygen pressure range of 130–150 bar, using a 5-kW xenon arc lamp as the illumination source.

B. Calculation of superconducting volume fraction

Following the approach outlined in Ref. [17], we calculated the superconducting volume fraction of $Pr_4Ni_3O_{10}$. The sample was a flat cylinder with a diameter of 210 μm and a thickness of 25 μm. The demagnetizing factor N for this cylinder with an axial magnetic field was approximately 0.84 (Ref. [44]).

Using the refined lattice parameters obtained from XRD results, we computed the sample's volume at high pressure. The magnetic susceptibility in SI units was then calculated with the following equation:

$$\chi_{SI} = 4\pi\chi_{CGS} = \frac{4\pi\mu}{HV},$$

where μ denotes the measured magnetic moment at 5 K (after subtracting the constant background signal at the onset of T_c), and V represents the cell volume for an $I4/mmm$ primitive cell with $Z = 2$ at high pressure.

After correcting for the demagnetizing factor, the susceptibility χ is approximately -0.85 at 40.2 GPa and -0.88 at 49.5 GPa for sample $S3$, corresponding to superconducting volume fractions of 85% and 88%, respectively.

C. *In situ* high-pressure synchrotron x-ray diffraction measurement

The high-pressure XRD measurements were conducted at the beamline BL17UM of the Shanghai Synchrotron Radiation Facility with a wavelength of 0.4834Å. The experiments utilized a symmetric DAC with 300-μm culet-sized anvils and rhenium gaskets. Helium was used as the pressure-transmitting medium to ensure optimal hydrostatic conditions.

Note added. Recently, three independent studies reported signatures of superconductivity in $Pr_4Ni_3O_{10}$ [45–47]. However, none of these studies observed zero resistance, and the onset T_c values are also lower than those observed in our samples.

DATA AVAILABILITY

The data that support the findings of this article are not publicly available because of legal restrictions preventing unrestricted public distribution. The data are available from the authors upon reasonable request.

---

[1] P. A. Lee, N. Nagaosa, and X.-G. Wen, *Doping a Mott insulator: Physics of high-temperature superconductivity*, Rev. Mod. Phys. **78**, 17 (2006).

[2] D. J. Scalapino, *A common thread: The pairing interaction for unconventional superconductors*, Rev. Mod. Phys. **84**, 1383 (2012).

[3] Y. Kamihara *et al.*, *Iron-based layered superconductor* $La[O_{1-x}F_x]FeAs(x = 0.05–0.12)$ *with Tc = 26 K*, J. Am. Chem. Soc. **130**, 3296 (2008).

[4] J. G. Bednorz and K. A. Müller, *Possible high-T_c superconductivity in the* $Ba − La − Cu − O$ *system*, Z. Phys. B **64**, 189 (1986).

[5] Y. Maeno *et al.*, *Superconductivity in a layered perovskite without copper*, Nature (London) **372**, 532 (1994).

[6] F. Wang and T. Senthil, *Twisted Hubbard model for* Sr_2IrO_4: *Magnetism and possible high temperature superconductivity*, Phys. Rev. Lett. **106**, 136402 (2011).

[7] V. Anisimov, D. Bukhvalov, and T. Rice, *Electronic structure of possible nickelate analogs to the cuprates*, Phys. Rev. B **59**, 7901 (1999).

[8] D. Li *et al.*, *Superconductivity in an infinite-layer nickelate*, Nature (London) **572**, 624 (2019).

[9] H. Sun *et al.*, *Signatures of superconductivity near 80K in a nickelate under high pressure*, Nature (London) **621**, 493 (2023).

[10] Y. Zhang *et al.*, *High-temperature superconductivity with zero resistance and strange-metal behaviour in* $La_3Ni_2O_{7-\delta}$, Nat. Phys. **20**, 1269 (2024).

[11] N. Wang *et al.*, *Bulk high-temperature superconductivity in pressurized tetragonal* $La_2PrNi_2O_7$, Nature (London) **634**, 579 (2024).

[12] M. Wang *et al.*, *Normal and superconducting properties of* $La_3Ni_2O_7$, Chin. Phys. Lett. **41**, 077402 (2024).

[13] Y. Zhou *et al.*, *Evidence of filamentary superconductivity in pressurized* $La_3Ni_2O_7$ *single crystals*, Matter Radiat. Extremes **10**, 027801 (2025).

[14] G. Wang *et al.*, *Pressure-induced superconductivity in polycrystalline* $La_3Ni_2O_{7-\delta}$, Phys. Rev. X **14**, 011040 (2024).

[15] Z. Dong *et al.*, *Visualization of oxygen vacancies and self-doped ligand holes in* $La_3Ni_2O_{7-\delta}$, Nature (London) **630**, 847 (2024).

[16] X. Zhou *et al.*, *Revealing nanoscale structural phase separation in* $La_3Ni_2O_7$ *single crystal via scanning near-field optical microscopy*, arXiv:2410.06602.

[17] Y. Zhu *et al.*, *Superconductivity in pressurized trilayer* $La_4Ni_3O_{10-\delta}$ *single crystals*, Nature (London) **631**, 531 (2024).

[18] B. Scott *et al.*, *Layer dependence of the superconducting transition temperature of* $HgBa_2Ca_{n-1}CunO_{2n+2+\delta}$, Physica (Amsterdam) **230C**, 239 (1994).

[19] I. Kuzemskaya, A. Kuzemsky, and A. Cheglokov, *Superconducting properties of the family of mercurocuprates and role of layered structure*, J. Low Temp. Phys. **118**, 147 (2000).

[20] A. Iyo *et al.*, T_c *vs n relationship for multilayered high-T_c superconductors*, J. Phys. Soc. Jpn. **76**, 094711 (2007).

[21] Q. Li *et al.*, *Signature of superconductivity in pressurized* $La_4Ni_3O_{10}$, Chin. Phys. Lett. **41**, 017401 (2024).

[22] M. Zhang *et al.*, *Superconductivity in trilayer nickelate* $La_4Ni_3O_{10}$ *under pressure*, Phys. Rev. X **15**, 021005 (2025).

[23] H. Sakakibara *et al.*, *Theoretical analysis on the possibility of superconductivity in the trilayer Ruddlesden-Popper nickelate* $La_4Ni_3O_{10}$ *under pressure and its experimental examination: Comparison with* $La_3Ni_2O_7$, Phys. Rev. B **109**, 144511 (2024).

[24] Y. Zhang *et al.*, *Trends in electronic structures and* $s_\pm$ *wave pairing for the rare-earth series in bilayer nickelate superconductor* $R_3Ni_2O_7$, Phys. Rev. B **108**, 165141 (2023).

[25] Z. Pan *et al.*, *Effect of rare-earth element substitution in superconducting* $R_3Ni_2O_7$ *under pressure*, Chin. Phys. Lett. **41**, 087401 (2024).

[26] See Supplemental Material at http://link.aps.org/supplemental/10.1103/PhysRevX.15.021008 for [brief description].

[27] J. Zhang *et al.*, *High oxygen pressure floating zone growth and crystal structure of the metallic nickelates* $R_4Ni_3O_{10}(R = La, Pr)$, Phys. Rev. Mater. **4,** 083402 (2020).

[28] J. Song *et al.*, *Structure, electrical conductivity and oxygen transport properties of Ruddlesden-Popper phases* $Ln_{n+1}Ni_nO_{3n+1}$ *(Ln = La, Pr, and Nd; n = 1, 2, and 3)*, J. Mater. Chem. **8,** 22206 (2020).

[29] A. M. Samarakoon *et al.*, *Bootstrapped dimensional crossover of a spin density wave*, Phys. Rev. X **13,** 041018 (2023).

[30] Y. Shen *et al.*, *Structural and magnetic phase diagram of CrAs and its relationship with pressure-induced superconductivity*, Phys. Rev. B **93,** 060503(R) (2016).

[31] G. Stewart, *Superconductivity in iron compounds*, Rev. Mod. Phys. **83,** 1589 (2011).

[32] Q. Qin, J. Wang, and Y.-f. Yang, *Frustrated superconductivity in the trilayer nickelate* $La_4Ni_3O_{10}$, Innovat. Mater. **2,** 100102 (2024).

[33] H. LaBollita *et al.*, *Electronic structure and magnetic tendencies of trilayer* $La_4Ni_3O_{10}$ *under pressure: Structural transition, molecular orbitals, and layer differentiation*, Phys. Rev. B **109,** 195151 (2024).

[34] J.-X. Wang *et al.*, *Non-Fermi liquid and Hund correlation in* $La_4Ni_3O_{10}$ *under high pressure*, Phys. Rev. B **109,** 165140 (2024).

[35] Z. Huo *et al.*, *Electronic correlations and Hund's rule coupling in trilayer nickelate* $La_4Ni_3O_{10}$, arXiv:2407.00327.

[36] C.-Q. Chen *et al.*, *Trilayer multiorbital models of* $La_4Ni_3O_{10}$, Phys. Rev. B **110,** 014503 (2024).

[37] Y. Zhang *et al.*, *Prediction of $s_\pm$ wave superconductivity enhanced by electronic doping in trilayer nickelates* $La_4Ni_3O_{10}$ *under pressure*, Phys. Rev. Lett. **133,** 136001 (2024).

[38] H. Oh, B. Zhou, and Y.-H. Zhang, *Type II t-J model in charge transfer regime in bilayer* $La_3Ni_2O_7$ *and trilayer* $La_4Ni_3O_{10}$, Phys. Rev. B **111,** 020504 (2025).

[39] I. Leonov, *Electronic structure and magnetic correlations in the trilayer nickelate superconductor* $La_4Ni_3O_{10}$ *under pressure*, Phys. Rev. B **109,** 235123 (2024).

[40] J. Huang and T. Zhou, *Interlayer pairing-induced partially gapped Fermi surface in trilayer* $La_4Ni_3O_{10}$ *superconductors*, Phys. Rev. B **110,** L060506 (2024).

[41] Q.-G. Yang *et al.*, *Effective model and $s_\pm$ wave superconductivity in trilayer nickelate* $La_4Ni_3O_{10}$, Phys. Rev. B **109,** L220506 (2024).

[42] G. Zhou *et al.*, *Ambient-pressure superconductivity onset above 40 K in bilayer nickelate ultrathin films*, arXiv:2412.16622.

[43] E. K. Ko *et al.*, *Signatures of ambient pressure superconductivity in thin film* $La_3Ni_2O_7$, Nature (London), **638,** 935 (2024).

[44] R. Prozorov and V. G. Kogan, *Effective demagnetizing factors of diamagnetic samples of various shapes*, Phys. Rev. Appl. **10,** 014030 (2018).

[45] X. Huang *et al.*, *Signature of superconductivity in pressurized trilayer-nickelate* $Pr_4Ni_3O_{10-\delta}$, Chin. Phys. Lett. **41,** 127403 (2024).

[46] X. Chen *et al.*, *Non-bulk superconductivity in* $Pr_4Ni_3O_{10}$ *single crystals under pressure*, arXiv:2410.10666.

[47] C. Pei *et al.*, *Pressure-induced superconductivity in* $Pr_4Ni_3O_{10}$ *single crystals*, arXiv:2411.08677.